

Search for active neutrino disappearance using neutral-current interactions in the MINOS long-baseline experiment

P. Adamson,⁹ C. Andreopoulos,²¹ K. E. Arms,¹⁷ R. Armstrong,¹² D. J. Auty,²⁵ D. S. Ayres,¹ C. Backhouse,¹⁹ B. Baller,⁹ G. Barr,¹⁹ W. L. Barrett,³⁰ B. R. Becker,¹⁷ A. Belias,²¹ R. H. Bernstein,⁹ D. Bhattacharya,²⁰ M. Bishai,⁴ A. Blake,⁶ G. J. Bock,⁹ J. Boehm,¹⁰ D. J. Boehnlein,⁹ D. Bogert,⁹ C. Bower,¹² E. Buckley-Geer,⁹ S. Cavanaugh,¹⁰ J. D. Chapman,⁶ D. Cherdack,²⁸ S. Childress,⁹ B. C. Choudhary,⁹ J. H. Cobb,¹⁹ S. J. Coleman,³¹ A. J. Culling,⁶ J. K. de Jong,¹¹ M. Dierckxsens,⁴ M. V. Diwan,⁴ M. Dorman,^{16,21} S. A. Dytman,²⁰ C. O. Escobar,⁷ J. J. Evans,^{16,19} E. Falk Harris,²⁵ G. J. Feldman,¹⁰ M. V. Frohne,³ H. R. Gallagher,²⁸ A. Godley,²³ M. C. Goodman,¹ P. Gouffon,²² R. Gran,¹⁸ E. W. Grashorn,¹⁷ N. Grossman,⁹ K. Grzelak,^{29,19} A. Habig,¹⁸ D. Harris,⁹ P. G. Harris,²⁵ J. Hartnell,^{25,21} R. Hatcher,⁹ K. Heller,¹⁷ A. Himmel,⁵ A. Holin,¹⁶ L. Hsu,⁹ J. Hylen,⁹ G. M. Irwin,²⁴ M. Ishitsuka,¹² D. E. Jaffe,⁴ C. James,⁹ D. Jensen,⁹ T. Kafka,²⁸ S. M. S. Kasahara,¹⁷ J. J. Kim,²³ M. S. Kim,²⁰ G. Koizumi,⁹ S. Kopp,²⁷ M. Kordosky,^{31,16} D. J. Koskinen,¹⁶ S. K. Kotelnikov,¹⁴ A. Kreymer,⁹ S. Kumaratunga,¹⁷ K. Lang,²⁷ J. Ling,²³ P. J. Litchfield,¹⁷ R. P. Litchfield,¹⁹ L. Loiacono,²⁷ P. Lucas,⁹ J. Ma,²⁷ W. A. Mann,²⁸ A. Marchionni,⁹ M. L. Marshak,¹⁷ J. S. Marshall,⁶ N. Mayer,¹² A. M. McGowan,^{1,17} J. R. Meier,¹⁷ M. D. Messier,¹² C. J. Metelko,²¹ D. G. Michael,^{5,*} W. H. Miller,¹⁷ S. R. Mishra,²³ C. D. Moore,⁹ J. Morfin,⁹ L. Mualem,⁵ S. Mufson,¹² S. Murgia,²⁴ J. Musser,¹² D. Naples,²⁰ J. K. Nelson,³¹ H. B. Newman,⁵ R. J. Nichol,¹⁶ T. C. Nicholls,²¹ J. P. Ochoa-Ricoux,⁵ W. P. Oliver,²⁸ R. Ospanov,²⁷ J. Paley,¹² V. Paolone,²⁰ A. Para,⁹ T. Patzak,⁸ Ž. Pavlović,²⁷ G. Pawloski,²⁴ G. F. Pearce,²¹ C. W. Peck,⁵ D. A. Petyt,¹⁷ R. Pittam,¹⁹ R. K. Plunkett,⁹ A. Rahaman,²³ R. A. Rameika,⁹ T. M. Rauffer,²¹ B. Rebel,⁹ J. Reichenbacher,¹ P. A. Rodrigues,¹⁹ C. Rosenfeld,²³ H. A. Rubin,¹¹ V. A. Ryabov,¹⁴ M. C. Sanchez,^{1,10} N. Saoulidou,⁹ J. Schneps,²⁸ P. Schreiner,³ P. Shanahan,⁹ W. Smart,⁹ C. Smith,¹⁶ A. Sousa,¹⁹ B. Speakman,¹⁷ P. Stamoulis,² M. Strait,¹⁷ N. Tagg,²⁸ R. L. Talaga,¹ M. A. Tavera,²⁵ J. Thomas,¹⁶ M. A. Thomson,⁶ J. L. Thron,¹ G. Tinti,¹⁹ I. Trostin,¹³ V. A. Tsarev,¹⁴ G. Tzanakos,² J. Urheim,¹² P. Vahle,^{31,16} B. Viren,⁴ D. R. Ward,⁶ M. Watabe,²⁶ A. Weber,¹⁹ R. C. Webb,²⁶ A. Wehmann,⁹ N. West,¹⁹ C. White,¹¹ S. G. Wojcicki,²⁴ D. M. Wright,¹⁵ T. Yang,²⁴ K. Zhang,⁴ and R. Zwaska⁹

(The MINOS Collaboration)

¹Argonne National Laboratory, Argonne, Illinois 60439, USA

²Department of Physics, University of Athens, GR-15771 Athens, Greece

³Physics Department, Benedictine University, Lisle, Illinois 60532, USA

⁴Brookhaven National Laboratory, Upton, New York 11973, USA

⁵Lauritsen Laboratory, California Institute of Technology, Pasadena, California 91125, USA

⁶Cavendish Laboratory, University of Cambridge, Madingley Road, Cambridge CB3 0HE, United Kingdom

⁷Universidade Estadual de Campinas, IF-UNICAMP, CP 6165, 13083-970, Campinas, SP, Brazil

⁸APC – Université Paris 7 Denis Diderot, 10, rue Alice Domon et Léonie Duquet, F-75205 Paris Cedex 13, France

⁹Fermi National Accelerator Laboratory, Batavia, Illinois 60510, USA

¹⁰Department of Physics, Harvard University, Cambridge, Massachusetts 02138, USA

¹¹Physics Division, Illinois Institute of Technology, Chicago, Illinois 60616, USA

¹²Indiana University, Bloomington, Indiana 47405, USA

¹³High Energy Experimental Physics Department, ITEP, B. Chermushkinskaya, 25, 117218 Moscow, Russia

¹⁴Nuclear Physics Department, Lebedev Physical Institute, Leninsky Prospekt 53, 119991 Moscow, Russia

¹⁵Lawrence Livermore National Laboratory, Livermore, California 94550, USA

¹⁶Department of Physics and Astronomy, University College London, Gower Street, London WC1E 6BT, United Kingdom

¹⁷University of Minnesota, Minneapolis, Minnesota 55455, USA

¹⁸Department of Physics, University of Minnesota – Duluth, Duluth, Minnesota 55812, USA

¹⁹Subdepartment of Particle Physics, University of Oxford, Oxford OX1 3RH, United Kingdom

²⁰Department of Physics and Astronomy, University of Pittsburgh, Pittsburgh, Pennsylvania 15260, USA

²¹Rutherford Appleton Laboratory, Chilton, Didcot, Oxfordshire, OX11 0QX, United Kingdom

²²Instituto de Física, Universidade de São Paulo, CP 66318, 05315-970, São Paulo, SP, Brazil

²³Department of Physics and Astronomy, University of South Carolina, Columbia, South Carolina 29208, USA

²⁴Department of Physics, Stanford University, Stanford, California 94305, USA

²⁵Department of Physics and Astronomy, University of Sussex, Falmer, Brighton BN1 9QH, United Kingdom

²⁶Physics Department, Texas A&M University, College Station, Texas 77843, USA

²⁷Department of Physics, University of Texas at Austin, 1 University Station C1600, Austin, Texas 78712, USA

²⁸Physics Department, Tufts University, Medford, Massachusetts 02155, USA

²⁹Department of Physics, Warsaw University, Hoza 69, PL-00-681 Warsaw, Poland

³⁰Physics Department, Western Washington University, Bellingham, Washington 98225, USA

³¹Department of Physics, College of William & Mary, Williamsburg, Virginia 23187, USA

(Dated: August 14, 2019)

We report the first detailed comparisons of the rates and spectra of neutral-current neutrino interactions at two widely separated locations. A depletion in the rate at the far site would indicate mixing between ν_μ and a sterile particle. No anomalous depletion in the reconstructed energy spectrum is observed. Assuming oscillations occur at a single mass-squared splitting, a fit to the neutral- and charged-current energy spectra limits the fraction of ν_μ oscillating to a sterile neutrino to be below 0.68 at 90% confidence level. A less stringent limit due to a possible contribution to the measured neutral-current event rate at the far site from ν_e appearance at the current experimental limit is also presented.

PACS numbers: 14.60.St, 14.60.Pq

Several experiments observing charged-current interactions of neutrinos have provided compelling evidence for ν_μ and ν_e disappearance as the neutrinos propagate from the point of production [1, 2, 3, 4, 5]. The Super-Kamiokande experiment has reported extensively on the disappearance of ν_μ produced in the atmosphere [2]. Measurements of solar ν_e showed that the disappearance of those neutrinos is due to matter enhanced conversions [3]. The KamLAND reactor experiment provided clear evidence for $\bar{\nu}_e$ mixing [4].

These results are conventionally interpreted as mixing among the active neutrino flavors that couple to the electroweak current. Precise measurements of the Z boson decay width indicate there are only three light active neutrinos [6], but they do not exclude the existence of “sterile” neutrinos, ν_s , that do not couple to the electroweak current. Sterile neutrinos could help resolve several outstanding problems in particle physics and astrophysics. For example, sterile neutrinos with masses at the eV energy scale can participate in the seesaw mechanism to introduce neutrino masses [7] and can also aid in heavy element nucleosynthesis in supernovae [8]. The SNO experiment has shown that the total flux of active neutrinos from the Sun agrees with the expectation from solar models [9], thereby limiting the extent to which the first or second neutrino mass eigenstates could couple to a sterile neutrino. While the Super-Kamiokande experiment excludes pure $\nu_\mu \rightarrow \nu_s$ and favors pure $\nu_\mu \rightarrow \nu_\tau$ oscillations in its analysis of atmospheric neutrinos, an admixture of the two possibilities is allowed [10] and has attracted considerable attention in the literature [11].

The MINOS experiment has reported a significant deficit of ν_μ at its far detector relative to the near detector through measurement of the rate of ν_μ charged-current (CC) interactions [5, 12]. If this deficit is due solely to conversions of ν_μ to $\nu_\tau + \nu_e$, then the rate of neutral-current (NC) interactions at the far detector remains unchanged from the non-oscillation prediction. Alternatively, if any ν_μ convert to a sterile state, then the NC rate would be suppressed and the reconstructed energy spectrum would be distorted. In this Letter we report the first measurement of the total active neutrino rate using a precisely known long baseline and neutrinos

produced with an accelerator. The reconstructed energy spectra for NC and CC interactions are used to limit the fraction of ν_μ converting to ν_s by fitting them to a model of oscillations between ν_μ, ν_τ, ν_e , and ν_s dominated by the atmospheric mass-squared splitting.

The neutrino beam is produced using 120 GeV/ c protons from the Fermilab Main Injector incident on a graphite target, which is followed by two magnetic focussing horns. The neutrino energy spectrum can be changed by adjusting the horn current or the position of the target relative to the horns. The flavor composition of the beam is 92.9% ν_μ , 5.8% $\bar{\nu}_\mu$, and 1.3% $\nu_e + \bar{\nu}_e$. In this analysis the ν and $\bar{\nu}$ are assumed to oscillate with the same parameters. The data used in this analysis come from the low energy beam configuration whose peak neutrino energy is 3.3 GeV [5, 12], with an exposure of the far detector to 2.46×10^{20} protons on target.

The MINOS near detector is located 1.04 km downstream of the target, has a mass of 0.98 kt, and lies 103 m underground at Fermilab. The far detector is 734 km downstream of the near detector, has a mass of 5.4 kt, and is located in the Soudan Underground Laboratory in Minnesota, 705 m below the surface. The fiducial masses used for the near and far detectors are 27 t and 3.8 kt respectively.

The MINOS detectors are steel scintillator tracking calorimeters [13]. The vertically oriented detector planes are composed of 2.54 cm thick steel and 1 cm thick plastic scintillator. The scintillator layer is comprised of 4.1 cm wide strips with each strip coupled via wavelength-shifting fiber to one pixel of a multi-anode photo-multiplier tube [14, 15]. The near(far) detector is magnetized to an average toroidal field of 1.3(1.4) T.

Hadronic showers resulting from NC interactions generate scintillation light in an average of 12 strips for 1 GeV of deposited energy. Events must have at least 4 strips with signal in order to be considered in the analysis. Individual scintillator strips are grouped into either reconstructed tracks or showers, which are combined into events. The vertex for each event is required to be sufficiently far from any edge of the detector to ensure that the final-state hadronic showers are well contained within the fully sampled portion of the detectors.

The near detector data are used to predict the number of expected events in the far detector, but the ability to make this prediction is complicated by the high rate environment at the near detector. At an intensity of 2.2×10^{13}

*Deceased.

protons on target, an average of 16 neutrino interactions are produced in the near detector for each spill [5]. The reconstruction program separates individual neutrino interactions that occur within the same spill. This initial pass overestimates the number of NC interactions having reconstructed energy, $E_{\text{reco}} < 1$ GeV by 36%. Additional selections making use of event topology and timing are then used to decrease this background. Events must be separated by at least 40 ns, and events that occur within 120 ns of each other must have vertices separated by at least 1 m in the longitudinal direction [16]. After applying these criteria, the remaining background from poorly reconstructed events with $E_{\text{reco}} < 1$ GeV is 7%.

The rate of neutrino interactions from the neutrino beam in the far detector is much lower than in the near detector, with approximately 1 interaction for every 10^4 spills. Interactions from the beam neutrinos are identified using a window around the GPS time stamp of the spills of $-2 \mu\text{s} < t < 12 \mu\text{s}$ where $t = 0$ is the expected start time at the far detector of the $10 \mu\text{s}$ spill. Given the low rate of neutrino interactions in the far detector, spurious events that are coincident with the beam spills from noise, cosmic-ray muons, or poor event reconstruction can introduce backgrounds to the analysis. Additional criteria are used to remove such events, leaving a residual background of $< 1\%$ of the signal [17].

Charged-current interactions are identified by the presence of a track that may or may not be associated with a shower. Neutral-current interactions typically have a single hadronic shower, although the reconstruction may identify a track in the event; such tracks could come from pions, but are mostly reconstruction artifacts. An event is classified as NC-like if it has a reconstructed shower, is shorter than 60 planes, and has no track extending more than 5 consecutive planes beyond the shower [18]. Distributions of these event-topology parameters for near detector events are shown in Fig. 1. The principal background in the spectrum of NC-like events comes from highly inelastic ν_μ -CC interactions. The E_{reco} spectrum of NC-like events in the near detector is shown in Fig. 2. The distributions in Figs. 1 and 2 show good agreement between the data and Monte Carlo simulation.

The Monte Carlo simulation is used to make an initial estimate of the ratio of event yields in the far and near detectors as a function of E_{reco} . This ratio is multiplied by the observed energy spectrum in the near detector to produce a far detector prediction of the NC-like event spectrum. The true energy of the simulated neutrinos in each reconstructed energy bin of the prediction is used to determine the effect of oscillations for that range of reconstructed energy. To avoid biases, the methods for identifying NC-like events and predicting the far detector spectrum were developed and tested using only the near detector data and Monte Carlo simulation, and the analysis procedures were finalized prior to examining data in the far detector.

Figure 3 shows the measured and predicted E_{reco} spectra at the far detector. The spectra are compared using

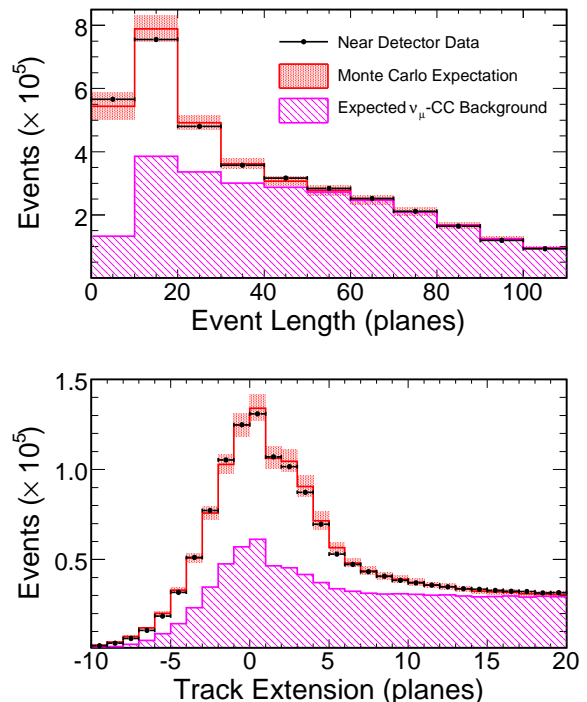


FIG. 1: Distributions of event-topology parameters used to separate NC-like from CC-like events. Data from the near detector (solid points) are shown superposed on the total Monte Carlo expectation. The hatched distribution shows the ν_μ -CC background as determined by the Monte Carlo simulation. The systematic uncertainty for the Monte Carlo expectation is shown by the shaded band.

a statistic, R , which expresses the agreement between the predicted and observed number of events in the far detector:

$$R \equiv \frac{N_{\text{Data}} - B_{\text{CC}}}{S_{\text{NC}}}, \quad (1)$$

where, within a given energy range, N_{Data} is the measured event count, B_{CC} is the extrapolated CC background from all flavors, and S_{NC} is the extrapolated number of NC interactions. The values of S_{NC} and contributions to B_{CC} are calculated in the framework of three neutrino oscillations and are shown in Table I. Because the disappearance of ν_μ occurs mainly for true neutrino energies < 6 GeV [12], the data are separated into two samples. Events with $E_{\text{reco}} < 3$ GeV are grouped into a low-energy sample while events with $3 \text{ GeV} < E_{\text{reco}} < 120$ GeV are grouped into a high-energy sample. The median true neutrino energies of the low and high energy samples are 3.1 GeV and 7.9 GeV respectively. The values of R calculated for these ranges in E_{reco} are shown in Table I. In the region with $E_{\text{reco}} < 3$ GeV, R differs from 1 by 1.3σ . Over the full energy range, $0 - 120$ GeV, the depletion of the total NC event rate is limited to be below 17% at 90% confidence level.

The principal sources of systematic uncertainty in R

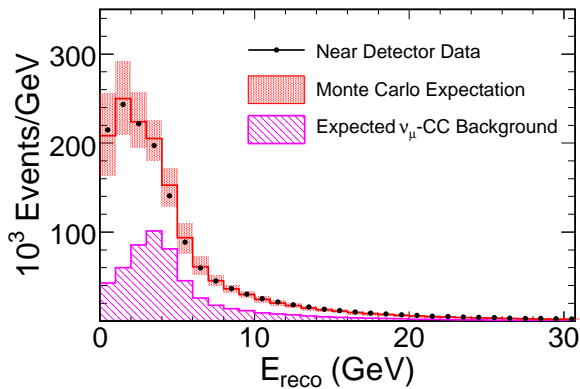


FIG. 2: The reconstructed energy spectrum for NC-like events in the near detector. The data (solid points) and the Monte Carlo expectation including systematic uncertainties (solid histogram with shaded band) are shown. The hatched distribution shows the expected ν_μ -CC background.

TABLE I: Values of N_{Data} , S_{NC} , and the contributions to B_{CC} for various reconstructed energy ranges. Also shown are the values of R . The numbers in parentheses are calculated including ν_e appearance at the upper limit discussed in the text.

E_{reco} (GeV)	N_{Data}	S_{NC}	$B_{\text{CC}}^{\nu_\mu}$	$B_{\text{CC}}^{\nu_\tau}$	$B_{\text{CC}}^{\nu_e}$
0 – 3	100	101.1	11.2	1.0	1.8 (9.3)
3 – 120	191	98.0	64.2	3.5	11.8 (24.6)
0 – 3	$R = 0.85 \pm 0.10 \pm 0.07$ (0.78 \pm 0.10 \pm 0.07)				
3 – 120	$R = 1.14 \pm 0.14 \pm 0.10$ (1.02 \pm 0.14 \pm 0.10)				
0 – 120	$R = 0.99 \pm 0.09 \pm 0.07$ (0.90 \pm 0.09 \pm 0.08)				

are listed in Table II. The absolute scale of the hadronic energy is known to within 12%, of which 10% reflects uncertainties in the final-state interactions in the nucleus and 6% results from uncertainty in the detector response to single hadrons. The relative calibration of the hadronic energy between the two detectors has an uncertainty of 3% [5], and the relative normalization between the detectors has an uncertainty of 4%. The uncertainty in the near detector event count due to the selection criteria is 15% for $E_{\text{reco}} < 0.5$ GeV; 3% for events with $0.5 \text{ GeV} < E_{\text{reco}} < 1$ GeV; and is negligible for $E_{\text{reco}} > 1$ GeV. The effect of these uncertainties on R is shown in Table II.

The uncertainty on the size of the ν_μ -CC background was determined by comparing the near detector NC-like reconstructed energy spectrum from the low energy beam configuration used in this analysis with the spectra from three other beam configurations with higher average neutrino energy. In each reconstructed energy bin, i , of the low energy beam the total number of events is the sum of the NC and CC interactions, $N_i = \text{NC}_i + \text{CC}_i$. The quantity r_i^{NC} (r_i^{CC}) is defined as the ratio of the number of NC(CC) interactions in each energy bin in an alternate beam configuration to the corresponding number in the low energy beam configuration. The value of CC_i

TABLE II: Sources of systematic uncertainties considered in this analysis and their effect on R .

	0 – 3 GeV	3 – 120 GeV
Absolute E_{had}	$\pm < 0.01$	± 0.05
Relative E_{had}	± 0.03	± 0.04
Normalization	± 0.04	± 0.08
Near detector selection	± 0.02	–
ν_μ -CC background	± 0.03	± 0.01
Total:	± 0.07	± 0.10

can be calculated from the spectrum in another beam,

$$\text{CC}_i = \frac{r_i^{\text{NC}} N_i - N_i^A}{r_i^{\text{NC}} - r_i^{\text{CC}}}, \quad (2)$$

where N_i^A is the total number of events observed in the alternate beam configuration. The values of r_i^{NC} and r_i^{CC} are taken from the Monte Carlo simulation. The uncertainty in the ν_μ -CC background is taken as the difference between the uncertainty-weighted average value of CC_i measured using the different beam configurations and the value predicted by the Monte Carlo simulation. That difference is consistent within 15% for all reconstructed energies. The size of the ν_μ -CC background at the far detector depends on the parameters for $\nu_\mu \rightarrow \nu_\tau$ oscillations used in the prediction. The MINOS measured values of $\Delta m_{32}^2 = 2.43 \times 10^{-3} \text{ eV}^2/c^4$ and $\theta_{23} = \pi/4$ [12] were used for the prediction, and variations within the 1σ range of these parameters change the ν_μ -CC background in the far detector by less than 10%.

Because the selection criteria identify ν_e -CC interactions as NC-like with nearly 100% efficiency, the background from ν_e inherent in the beam and $\nu_\mu \rightarrow \nu_e$ oscillations is also considered. An upper limit for the ν_e -CC rate in the far detector was estimated using the normal mass hierarchy with $\theta_{12} = 0.61$ rad, $\theta_{13} = 0.21$ rad, $\delta = 3\pi/2$ rad, $\Delta m_{21}^2 = 7.59 \times 10^{-5} \text{ eV}^2/c^4$, and $\Delta m_{32}^2 = 2.43 \times 10^{-3} \text{ eV}^2/c^4$ [4, 12]. The choice of θ_{13} corresponds to the 90% confidence level upper limit for the chosen Δm_{32}^2 value [19]. The contribution to B_{CC} from ν_e and the values of R in the different energy ranges under these assumptions are shown in Table I.

The data shown in Fig. 3 can be combined with the data from CC interactions to determine whether the previously observed ν_μ disappearance is due solely to oscillations between the active neutrinos, or if oscillations between active and sterile neutrinos also occur. To determine the fraction of ν_μ that have converted to a sterile state, the data are fit to a model that assumes oscillations between ν_μ , ν_τ , and ν_s occur at a single mass-squared splitting. The probabilities for ν_μ to remain ν_μ or convert to ν_s are

$$\begin{aligned} P_{\nu_\mu \rightarrow \nu_\mu} &= 1 - \alpha_\mu \sin^2(1.27 \Delta m^2 L/E), \text{ and} \\ P_{\nu_\mu \rightarrow \nu_s} &= \alpha_s \sin^2(1.27 \Delta m^2 L/E), \end{aligned} \quad (3)$$

where Δm^2 is the atmospheric mass-squared splitting in

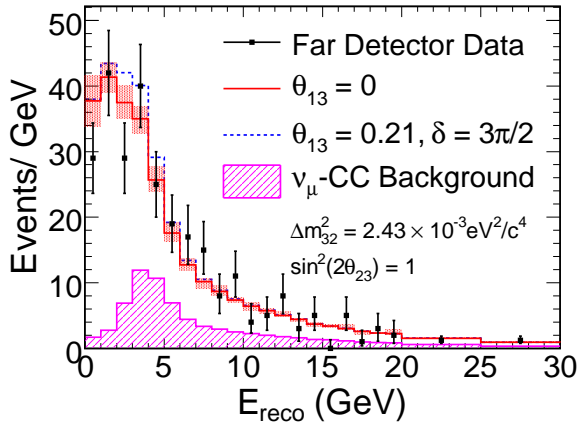


FIG. 3: Spectrum of observed NC-like events in the far detector with predictions for the two oscillation hypotheses described in the text. The filled regions in each bin indicates the systematic uncertainty in the predicted rates.

eV^2/c^4 , $L = 735$ km, E is the energy of the neutrino in GeV, and α_μ and α_s are phenomenological parameters related to the mixing angles. A simultaneous fit to the E_{reco} spectrum in Fig. 3 and the ν_μ -CC energy spectrum yields the energy independent fraction of ν_μ that oscillate to ν_s ,

$$f_s \equiv \frac{P_{\nu_\mu \rightarrow \nu_s}}{1 - P_{\nu_\mu \rightarrow \nu_\mu}} = 0.28^{+0.25}_{-0.28}(\text{stat.}+\text{syst.}), \quad (4)$$

with $\chi^2 = 46.5$ for 43 degrees of freedom and $f_s < 0.68$ at 90% confidence level. The fit includes the systematic uncertainties in Table II as nuisance parameters. Including electron neutrino appearance at the previously discussed upper limit results in $f_s = 0.43^{+0.23}_{-0.27}(\text{stat.}+\text{syst.})$ with $\chi^2 = 46.6$ and $f_s < 0.80$ at 90% confidence level.

In summary, we have reported the first measurements of neutrino neutral-current rates and spectra in an accelerator long baseline neutrino experiment. The rates at the near and far detectors are consistent with expectations from decay kinematics and geometry, providing new support for the interpretation of muon neutrino disappearance as oscillations among the three active neutrinos. This result provides the best limits to date on the fraction of muon neutrinos which may convert to sterile neutrinos in oscillations associated with the atmospheric mass-squared splitting.

This work was supported by the US DOE, the UK STFC, the US NSF, the State and University of Minnesota, the University of Athens, Greece, and Brazil's FAPESP and CNPq. We thank S. Parke for useful discussions. We are grateful to the Minnesota Department of Natural Resources, the crew of the Soudan Underground Laboratory, and the staff of Fermilab for their contribution to this effort.

-
- [1] R. Davis et al., Phys. Rev. Lett. **20**, 1205 (1968); R. Becker-Szendy et al., Phys. Rev. D **46**, 3720 (1992); K. S. Hirata et al., Phys. Lett. B **280**, 146 (1992); J. N. Abdurashitov et al., Phys. Lett. B **328**, 234 (1994); M. Sanchez et al., Phys. Rev. D **68**, 113004 (2003); M. H. Ahn et al., Phys. Rev. D **74**, 072003 (2006).
- [2] Y. Fukuda et al., Phys. Rev. Lett. **81**, 1562 (1998); Y. Ashie et al., Phys. Rev. Lett. **93**, 101801 (2004); Y. Ashie et al., Phys. Rev. D **71**, 112005 (2005).
- [3] P. Anselmann et al., Phys. Lett. B **285**, 376 (1992); J. N. Abdurashitov et al., Phys. Rev. Lett. B **328**, 234 (1994); Y. Fukuda et al., Phys. Rev. Lett. **86**, 5651 (2001); J. Hosaka et al., Phys. Rev. D **73**, 112001 (2006); Q. R. Ahmad et al., Phys. Rev. Lett. **89**, 011301 (2006).
- [4] S. Abe et al., Phys. Rev. Lett. **100**, 221803 (2008); T. Araki et al., Phys. Rev. Lett. **94**, 081801 (2005).
- [5] P. Adamson et al., Phys. Rev. D **77**, 072002 (2008).
- [6] M. Acciarri et al., Phys. Lett. B **431**, 199 (1998); P. Abreu et al., Z. Phys. **C74**, 577 (1997); R. Akers et al., Z. Phys **C65**, 47 (1995); D. Buskulic et al., Phys. Lett. B **313**, 520 (1993); G. S. Abrams et al., Phys. Rev. Lett **63**, 2173 (1989).
- [7] A. de Gouvea, J. Jenkins, and N. Vasudevan, Phys. Rev. D **75**, 013003 (2007), hep-ph/0608147.
- [8] G. C. McLaughlin et al., Phys. Rev. C **59**, 2873 (1999); D. O. Caldwell et al., Phys. Rev. D. **61**, 123005 (2000); J. Fetter et al., Astropart. Phys. **18**, 433 (2003).
- [9] Q. R. Ahmad et al., Phys. Rev. Lett. **89**, 011301 (2002), nucl-ex/0204008.
- [10] Y. Fukuda et al., Phys. Rev. Lett. **85**, 3999 (2000); K. Abe et al., Phys. Rev. Lett. **97**, 171801 (2006).
- [11] G. L. Fogli et al., Phys. Rev. D **64**, 093005 (2001); A. Donini et al. JHEP **12**, 013 (2007); A. Dighe and S. Ray, Phys. Rev. D **76**, 113001 (2007).
- [12] D. G. Michael et al., Phys. Rev. Lett. **97**, 191801 (2006); P. Adamson et al., Phys. Rev. Lett. **101** 131802 (2008).
- [13] D. G. Michael et al. (2008), *accepted to Nucl. Instrum. Meth.*, arXiv:0805.3170 [physics.ins-det].
- [14] N. Tagg et al., Nucl. Instrum. Meth. **A539**, 668 (2005).
- [15] K. Lang et al., Nucl. Instrum. Meth. **A545**, 852 (2005).
- [16] T. M. Raufer, Ph.D. Thesis, Oxford University (2007).
- [17] R. P. Litchfield, Ph.D. Thesis, Oxford University (2008).
- [18] T. Osiecki, Ph.D. Thesis, University of Texas at Austin (2007).
- [19] M. Apollonio et al., Eur. Phys. J. **C27**, 331 (2003), hep-ex/0301017.